Proceedings of the 21st ICSMGE, Vienna, Austria, 14 – 19 June 2026. Pistrol, Adam & Schweiger (eds.)
Published by: ÖGG, Austrian Society for Geomechanics, Salzburg, Austria, ISBN 978-3-9503898-4-5
https://doi.org/10.53243/ICSMGE2026-1333

Energy dissipation of clays during undrained cyclic triaxial tests

Francesca Palmieri, David M.G. Taborda
Department of Civil and Environmental Engineering, Imperial College London, United Kingdom,
f.palmieri@imperial.ac.uk

ABSTRACT: Experimentally, the cumulative dissipated energy, representing the energy dissipated over consecutive loading cycles, is recognised as a measure of damage induced by cyclic loading. This paper presents a bounding surface constitutive model for the cyclic loading response of clays, in which dissipated energy is introduced as an internal variable to reproduce cyclic degradation. The model's ability to simulate the cumulative dissipated energy and damping is evaluated through comparisons with experimental results from undrained cyclic triaxial tests. While generally good agreement between numerical and experimental datasets is observed, this study highlights limitations in predicting energy dissipation at large strains. Therefore, an enhancement to the formulation is proposed to improve model performance.

KEYWORDS: Energy dissipation, clays, constitutive modelling, cyclic loading, damage, damping.

1 INTRODUCTION

Under undrained cyclic loading conditions, clays exhibit non-linear hysteretic stress-strain response, with stiffness and damping dependent on the cyclic loading amplitude. At large strain amplitudes, stiffness progressively degrades with the number of cycles (N), along with increased energy dissipation and, consequently, greater damping. Accurate representation of this response, including its dependence on both amplitude and N, is important for practical applications across various fields, such as earthquake engineering and offshore geotechnics.

In finite element analyses, advanced constitutive models are required to capture key aspects of the undrained cyclic loading response of clays. Two main approaches are generally adopted, with the simplest being the development of models within the cyclic nonlinear elastic framework (Finn et al., 1977). These are effective in representing the dependence of stiffness and damping on the loading amplitude and can also account for the effect of N if a degradation law is added. Their formulation makes them particularly suited for wave propagation problems involving relatively simple loading paths, such as site response analyses. In contrast, models developed within the bounding surface (BS) plasticity framework (Dafalias and Herrmann, 1986) are more appropriate for a wider range of complex loading conditions, e.g., including monotonic phases, dissipation of excess pore water pressures, or soil-structure interaction. While each approach has its own strengths, neither works best across all applications. A common limitation of BS plasticity models is the overprediction of energy dissipation and damping at large strains (Elia and Rouainia, 2016, Eslami et al., 2019), which can lead to non-conservative assessments of soil performance under cyclic loading.

A novel constitutive model within the BS plasticity framework has been recently developed by Palmieri and Taborda (2025) for the cyclic response of clays. It builds on the SANICLAY family of models (Dafalias et al., 2006), which has demonstrated reliable predictions of complex soil behaviour under monotonic and cyclic loading (e.g., Rezania et al., 2018, Palmieri and Taiebat, 2024). The proposed formulation incorporates an energy-based degradation mechanism where damage evolves with dissipated energy and is activated when the energy dissipated by the material since the last reversal, referred to herein as the *cycle-specific dissipated energy*, exceeds a specified threshold. In practice, the evolution law uses the *effective cumulative dissipated energy*, defined as the cumulative value reduced by the activation threshold, so that only dissipation beyond this limit contributes to damage development. The presence of this energy threshold allows the model to account for the effect of N on stiffness and damping only at large cyclic amplitudes, thus reflecting the experimentally observed response of clays (Voznesensky and Nordal 1999, Okur and Ansal 2011). While a similar outcome was achieved by Palmieri and Taiebat (2024) with an alternative strain-driven degradation mechanism, the advantage of an energy-based damage variable is that its impact on the modelled behaviour is loading path independent, accounting simultaneously for cyclic stress, cyclic strain, and N using a single scalar quantity. Despite the many advantages associated with this novel damage mechanism, the proposed formulation appears to share the limitation of BS constitutive models in overpredicting energy dissipation at large strains. Palmieri and Taborda (2025) qualitatively acknowledged this overdamping, noting the lack of loop tightening in the final cycles when compared to experimental observations.

This paper quantifies the model's performance in terms of reproducing cumulative dissipated energy and damping in undrained cyclic triaxial tests, comparing the computed response to experimental results. The analysis reveals specific limitations, leading to a modified formulation, which is shown to have a substantial impact on the stress-strain response at large strains.

2 MODEL FORMULATION

The present model builds upon the BS SANICLAY framework, as formulated by Seidalinov and Taiebat (2014), where the plastic modulus K_p, which controls plastic strain evolution, depends on the distance between the current stress state, $\boldsymbol{\sigma}$, and its image on the BS, $\bar{\boldsymbol{\sigma}}$. This distance defines the non-dimensional distance ratio b, which affects K_p via:

$$K_\mathrm{p} = \bar{K}_\mathrm{p} + \frac{h p_0^3}{\langle b/(b-1) - s \rangle} \tag{1}$$

where $\bar{K}_\mathrm{p}$ is the plastic modulus at the image stress, h is a parameter controlling the rate of hardening, p_0 is the size of the BS, and $s \geq 1$ is a model parameter representing the size of the elastic nucleus. To establish the image stress, the model adopts a moving projection centre, which relocates at each reversal, the latter being identified by negative values of the loading index.

To predict cyclic degradation, a scalar damage variable d is adopted, which modifies h, and therefore K_p, as follows:

$$h = \frac{h_0}{1 + d} \tag{2}$$

In Equation (2), h_0 is the parameter defining the initial value of h.

While the reference SANICLAY accounts for cyclic degradation via a plastic strain-driven damage variable, here, damage evolves with dissipated energy. In this approach, the model continuously evaluates the dissipated energy during cyclic loading using the algorithm by Taborda et al. (2016), according to which the energy dissipated between the last reversal $(\boldsymbol{\varepsilon}_{\text{rev}}, \boldsymbol{\sigma}_{\text{rev}})$ and the current loading step i $(\boldsymbol{\varepsilon}_{\text{i}}, \boldsymbol{\sigma}_{\text{i}})$, is given by:

$$E_{\text{diss,i}} = E_{\text{acc,i}} - E_{\text{el,i}} \tag{3}$$

where the accumulated energy $E_{\text{acc,i}}$ and elastic energy $E_{\text{el,i}}$ are computed as:

$$E_{\text{acc,i}} = \int_{\boldsymbol{\varepsilon}_{rev}}^{\boldsymbol{\varepsilon}_i} (\boldsymbol{\sigma}_{\mathbf{i}} - \boldsymbol{\sigma}_{\text{rev}}) : d\boldsymbol{\varepsilon} \tag{4}$$

$$E_{\text{el,i}} = \frac{1}{2}(\boldsymbol{\sigma}_{\mathbf{i}} - \boldsymbol{\sigma}_{\text{rev}}) : (\boldsymbol{\varepsilon}_{\mathbf{i}} - \boldsymbol{\varepsilon}_{\text{rev}}) \tag{5}$$

Here, $\boldsymbol{\sigma}$ and $\boldsymbol{\varepsilon}$ are second-order stress and strain tensors, with subscripts i and rev referring to the current and reversal states, respectively; the colon (:) denotes the trace product.

The cycle-specific dissipated energy, E^*_{diss}, is obtained by summing $E_{\text{diss,i}}$ over all increments since the last reversal and is used to evaluate damage. Specifically, the evolution of damage is driven by the effective cumulative dissipated energy $E^{\text{eff}}_{\text{diss}}$ according to:

$$\dot{d} = {a_{\text{d}}}^{b} \dot{E}^{\text{eff}}_{\text{diss}} \tag{6}$$

where a_{d} is a parameter controlling the rate of evolution of d, and b is the abovementioned distance ratio, which introduces the effect of cyclic stress amplitude. The rate $\dot{E}^{\text{eff}}_{\text{diss}}$ is computed as:

$$\dot{E}^{\text{eff}}_{\text{diss}} = H\,(E^*_{\text{diss,max}} - E_{\text{a}}) \cdot \dot{E}_{\text{diss,i}} \tag{7}$$

where E_{a} is the activation energy threshold parameter and $H(\cdot)$ the Heaviside function, ensuring that damage initiates when E_{a} is exceeded. The activation is evaluated using the maximum cycle-specific dissipated energy $E^*_{\text{diss,max}}$ during loading history. Once E_{a} is exceeded, all subsequent dissipated-energy increments contribute to damage.

Finally, to improve the prediction of stiffness at very small strains, the formulation includes the empirical relation by Viggiani and Atkinson (1995) for the small-strain shear modulus G_0, which accounts for effective stress and OCR.

3 MODEL EVALUATION

The model is evaluated in terms of its ability to simulate energy dissipation and damping when used to model undrained cyclic triaxial tests at constant cyclic stress ratio (CSR), defined in this case as the cyclic shear stress normalized by the undrained shear strength s_u. Model parameters and initial conditions are taken from Palmieri and Taborda (2025), where the model was calibrated to reproduce the stress–strain response exhibited by destructured specimens of Cloverdale clay, including the observed cyclic stress threshold of CSR = 0.55, with s_u = 56 kPa (Zergoun and Vaid, 1994). This threshold marks the onset of major stiffness degradation and increasing energy dissipation with N. Tests were conducted with OCR = 1, void ratio e = 1.0, and isotropic confining pressure of 200 kPa. The adopted model parameters are summarised in Table 1.

Figure 1 presents the evolution of cumulative dissipated energy with N for different CSR values ranging from 0.27 to 0.79. In this and subsequent figures, N is evaluated at the zero-crossing of each cycle, i.e., when the average deviatoric stress $q_{\text{av}} = 0$. The results show that the rate of energy accumulation strongly depends on CSR. For CSRs below the threshold value of 0.55, the dissipated energy accumulates at a low rate, which decreases during the early stages of cyclic loading until reaching a relatively constant value that depends on CSR. This constant rate indicates that the response remains stable over repeated cycles, with the stress-strain loops not evolving significantly. In contrast, for CSR values above the threshold, the accumulation rate of dissipated energy sharply increases with N, reflecting the progressive degradation of stiffness and associated rotation of the hysteresis loops. These contrasting responses demonstrate the effect of the activation energy parameter, which controls the onset of damage evolution.

Table 1. Description of model parameters and calibrated values for Cloverdale clay.

Parameter		Value	Unit
A	Stiffness at small strains G_0	550.0	-
m	Pressure dependency of G_0	0.23	-
n	OCR dependency of G_0	0.77	-
p_{ref}	Reference pressure for G_0	1	kPa
λ	Slope of the compression line	0.21	-
κ	Slope of the swelling line	0.03	-
M_{c}	Stress ratio at CS in triaxial compression	1.29	-
M_{e}	Stress ratio at CS in triaxial extension	1.27	-
N	Shape factor for the bounding surface	1.0	-
C	Rate of evolution of anisotropy	3.0	-
x	Saturation limit of anisotropy	1.73	-
s	Size of elastic region	1.0	-
h_0	Hardening modulus parameter	200.0	-
a_{d}	Damage parameter	0.8	-
E_{a}	Activation energy	0.14	kJ/m³

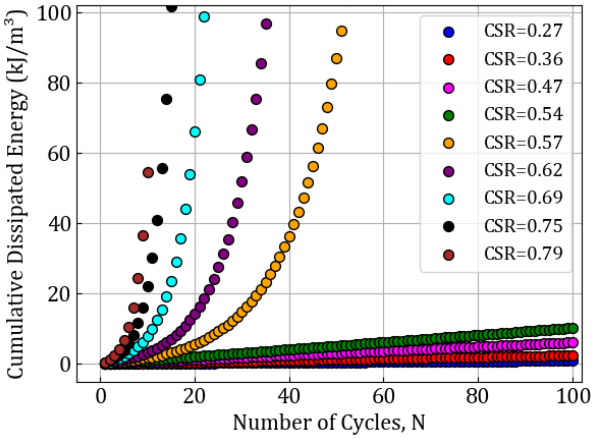

Figure 1. Prediction of cumulative dissipated energy with cycles under various CSRs.

Figure 2 compares the cumulative dissipated energy against peak-to-peak axial strain for different CSRs, with simulation results shown alongside the experimental data. In this plot, simulation data points correspond to specific numbers of cycles (N = 1, 5, 10, 20, 40, 60, 100), which may not directly match the experimental data, as this information was absent in the original reference. Results show that the model can reproduce the overall trend observed in the experiments. The best

agreement is found at smaller strains, while at larger strains, the model tends to overpredict the dissipated energy. Figure 3 further explains the results observed in Figure 2 by showing the corresponding damping ratios as a function of peak-to-peak axial strain. For each CSR, model predictions agree with the experimental values at small strains, mostly owing to the calibration of parameters E_a and h_0. However, at larger strains occurring for CSRs above the threshold, the model increasingly overestimates damping, as observed with other models employing a similar framework (Elia and Rouainia, 2016; Eslami et al., 2019). Since damping is directly related to the area within each stress-strain loop, the results in this plot demonstrate the model's tendency to overpredict cumulative energy dissipation at large strains. This specific shortcoming was already recognized in Palmieri and Taborda (2025), who highlighted the model's inability to capture the tightening of the hysteresis loops observed in experiments at CSRs above the threshold.

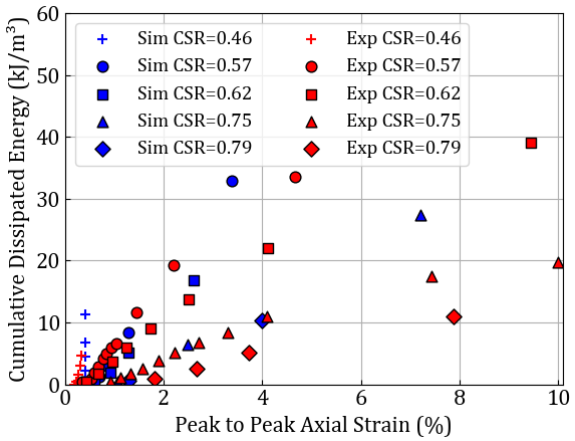

Figure 2. Prediction of cumulative dissipated energy under various CSRs and number of cycles in comparison with experiment.

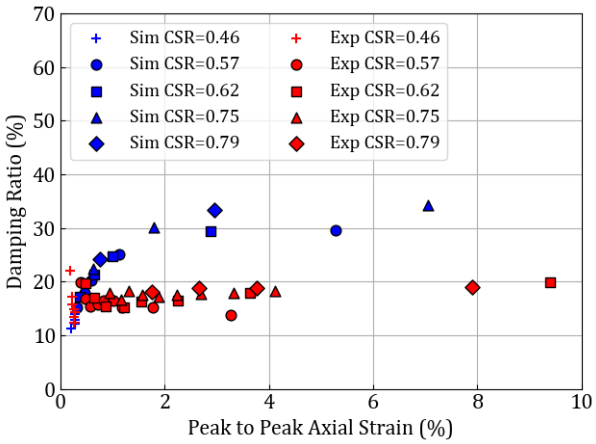

Figure 3. Prediction of damping under various CSRs and number of cycles in comparison with experiment.

4 MODEL ENHANCMENT

To address the overestimation of damping observed at large strains, a modification is introduced to the evolution of the parameter h, which controls K_p via Equation (1).

Following Palmieri and Taiebat (2024), the variable b_{sr} is defined as the value of b recorded at the last stress reversal. Figure 4 shows the evolution of b (Figure 4a), b_{sr} (Figure 4b), and b/b_{sr} (Figure 4c) during cyclic loading at CSR = 0.75. As discussed in Section 2, the variable b represents the non-dimensional distance ratio, which can assume values ≥ 1, with a value of 1 corresponding to stress states lying on the BS with stress and image stress coinciding. The variable b_{sr} is updated only at stress reversal, resulting in a stepwise evolution with constant value within each half-cycle, stabilising once hardening becomes less evident. The ratio b/b_{sr}, increases enormously upon stress reversal, gradually reducing towards unity during further shearing, until the next reversal occurs.

The proposed modification replaces Equation (2) with:

$$h = \frac{h_0}{1 + d\,\frac{b}{b_{sr}}} \tag{8}$$

where $b/b_{sr} \geq 1$. Upon stress reversal, b/b_{sr} becomes very large and h reduces, leading to narrower stress-strain loops and, hence, to lower damping ratio values. As shearing progresses within each half-cycle, b/b_{sr} reduces and h increases, thus limiting the stiffness reduction.

Figure 5 compares the stress-strain response at CSR = 0.75 obtained with the reference formulation (Figure 5a) and with the proposed evolution law (Figure 5b). Clearly, the use of Equation (8) produces slightly higher strain levels but tighter hysteresis loops, both of which lead to a reduction in simulated damping relative to the original version.

Finally, Figures 6 and 7 quantify the effect of the proposed modification on cumulative dissipated energy and damping ratio, respectively, for the same simulations presented in Figure 5. With the reference to Equation (2), energy dissipation increases rapidly with N, reaching values larger than 40 kJ/m³ at N = 12, while the damping ratio grows steadily from ~22 % to ~35 %. In contrast, the proposed Equation (8) reduces the rate of energy accumulation, resulting in ~30 kJ/m³ at N = 12, and stabilises the damping ratio at around 20 % after the first few cycles.

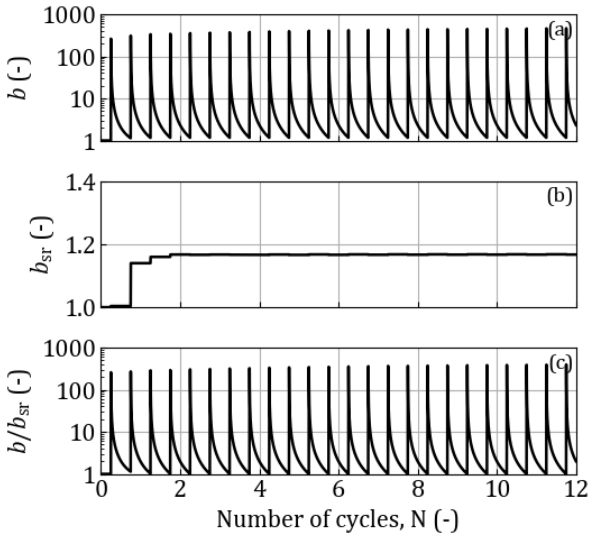

Figure 4. Evolution of variables during cyclic loading: b (a), b_{sr} (b), and b/b_{sr} (c).

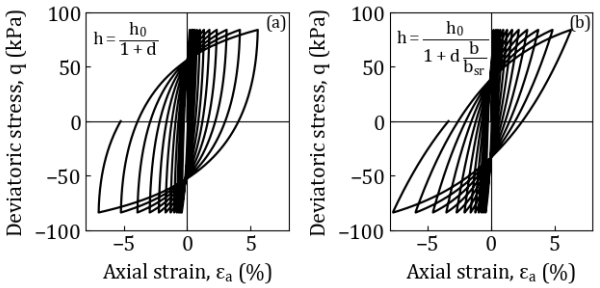

Figure 5. Stress-strain response at CSR= 0.75 with different evolution laws for h: (a) reference Equation (2), and (b) proposed Equation (8).

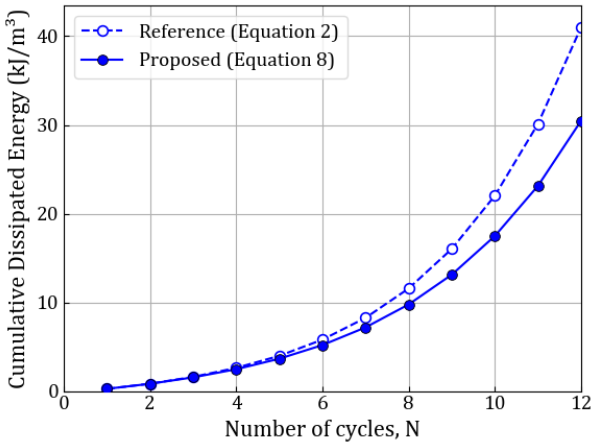

Figure 6. Evolution of cumulative dissipated energy at CSR = 0.75 for different evolution laws for h.

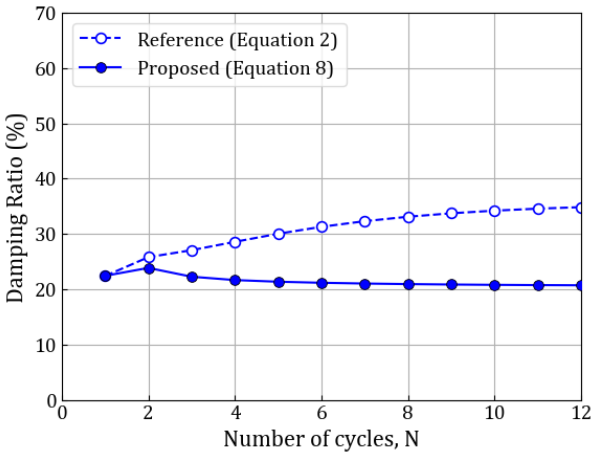

Figure 7. Evolution of damping ratio at CSR = 0.75 for different evolution laws for h.

5 CONCLUSIONS

The performance of a newly developed constitutive model for the cyclic loading behaviour of clays is assessed, with emphasis on its ability to reproduce energy dissipation during undrained cyclic triaxial tests at different CSR levels. The model, a SANICLAY formulation with bounding surface, features an energy-based degradation mechanism where damage evolves with dissipated energy and is activated when dissipation exceeds a specific threshold, allowing cyclic degradation to be reproduced only at large cyclic loading amplitudes. Concepts such as *cycle-specific dissipated energy* and *effective cumulative energy* are introduced to explain the novel damage mechanism.

Cloverdale clay, a material for which an extensive experimental database consisting of several undrained cyclic triaxial compression tests performed at a wide range of CSR values exists, was used to demonstrate the performance of the proposed formulation. Comparisons between simulated and experimental results show good agreement at small strains, where the model reproduces the observed damping and cumulative dissipated energy. At large strains, however, it overpredicts dissipation, a feature common to bounding surface plasticity models. To address this limitation, an alternative formulation for the plastic stiffness is proposed, using the non-dimensional stiffness ratio b, and its value at the last stress reversal to introduce a measure of stress amplitude with respect to the size of the bounding surface. The modified formulation is shown to yield slightly larger strains under the stress amplitude, suggesting an increase in elastic energy. Concurrently, the new expression results in tighter stress-strain loops, reducing the cyclic specific dissipated energy. Both effects result in a considerable reduction in damping ratio and therefore a much better agreement with observed experimental trends.

6 ACKNOWLEDGEMENTS

The authors gratefully acknowledge funding from the Royal Commission for the Exhibition of 1851.

7 REFERENCES

Dafalias, Y. F., and Herrmann, L. R. 1986. Bounding surface plasticity. II: Application to isotropic cohesive soils. *Journal of Engineering Mechanics*, 112(12), 1263-1291.

Dafalias, Y. F., Manzari, M. T., and Papadimitriou, A. G. 2006. SANICLAY: simple anisotropic clay plasticity model. *Int. J. Numer. Anal. Methods Geomech* 30(12), 1231-1257.

Elia, G., and Rouainia, M. 2016. Investigating the cyclic behaviour of clays using a kinematic hardening soil model. *Soil Dynamics and Earthquake Engineering*, 88, 399-411.

Eslami, M. M., Zarrabi, M., and Yniesta, S. 2019. Evaluation of two constitutive models in predicting cyclic behavior of a natural clay. *7th International Conference on Earthquake Geotechnical Engineering (ICEGE 2019)*, Rome, 2275-2282.

Finn, W. L., Lee, K. W., and Martin, G. R. 1977. An effective stress model for liquefaction. *Journal of the Geotechnical Engineering Division*, 103(6), 517-533.

Okur, V., and Ansal, A. 2011. Evaluation of cyclic behavior of fine-grained soils using the energy method. *Journal of Earthquake Engineering* 15(4), 601-619.

Palmieri, F., and Taborda, D. M. G. 2025. Modelling energy dissipation of clays during cyclic loading. *Proc. 17th International Conference of the International Association for Computer Methods and Advances in Geomechanics (IACMAG 2025)*, Hong Kong (in press).

Palmieri, F., and Taiebat, M. 2024. An activation mechanism for cyclic degradation of clays in bounding surface plasticity. *Int. J. Numer. Anal. Methods Geomech* 48(9), 2303-2319.

Rezania, M., Nguyen, H., Zanganeh, H., & Taiebat, M. 2018. Numerical analysis of Ballina test embankment on a soft structured clay foundation. *Computers and Geotechnics*, 93, 61-74.

Seidalinov, G., and Taiebat, M. 2014. Bounding surface SANICLAY plasticity model for cyclic clay behavior. *Int. J. Numer. Anal. Methods Geomech* 38(7), 702-724.

Taborda, D. M. G., Potts, D. M., and Zdravković, L. 2016. On the assessment of energy dissipated through hysteresis in finite element analysis. *Computers and Geotechnics* 71, 180-194.

Voznesensky, E. A., and Nordal, S. 1999. Dynamic instability of clays: an energy approach. *Soil dynamics and earthquake engineering* 18(2) 125-133.

Viggiani, G., and Atkinson, J. H. 1995. Stiffness of fine-grained soil at very small strains. *Géotechnique* 45(2), 249-265.

Zergoun, M., and Vaid, Y. P. 1994. Effective stress response of clay to undrained cyclic loading. *Canadian Geotechnical Journal* 31(5), 714-727.